

Study on the bearing capacity of cold-formed steel under different boundary conditions in transmission towers

Junke Han^{1,2a}, Xu Zhao^{1b}, Zhenyun Tang^{*1}, Hua Ma^{1c} and Zhenbao Li^{1d}

¹Beijing Key Lab of Earthquake Engineering and Structural Retrofit, Beijing University of Technology, Beijing, 100124, China

²China Electric Power Research Institute, Beijing 100055, China

(Received January 21, 2017, Revised April 28, 2017, Accepted May 26, 2017)

Abstract. Cold-formed steel is widely used in steel structures, especially in transmission towers, because of advantages such as low weight, high strength, excellent mechanical properties, etc. However, there is not a special design code for cold-formed steel use in transmission towers in China. For this study, a total of 105 compression members were tested statically to investigate the bearing capacity of cold-formed steel members under different boundary conditions in transmission towers. The test results were compared to the results predicted by the current design codes. For deeper insight, additional coupled members were simulated using finite element analysis. An improved design method was developed based on the experimental and analytical results.

Keywords: bearing capacity; instability; cold-formed steel; transmission tower; boundary condition

1. Introduction

More than 17000 km of new transmission lines are constructed every year in China (Yang *et al.* 2014 and Jiang *et al.* 2014). The performance of the transmission towers plays a very important role in ensuring that the transmission line system works well. Compared to conventional steel (Nashid *et al.* 2015 and Li *et al.* 2014), cold-formed steel has several advantages (e.g., low weight, high strength, and excellent mechanical properties), and it is widely used in transmission towers (Yang *et al.* 2011) and buildings (Shahi *et al.* 2013 and Rosario-Galanes and Godoy 2014). This weather resistant steel has been introduced into transmission towers to retard the strength reduction of the steel members, which is caused by environmental effects (Yang *et al.* 2009).

In a transmission tower, each cold-formed steel member affects the mechanical properties of the tower, while the performance of each steel member is determined by its stability (Kennedy and Murty 1972 and Bathon *et al.* 1993). Therefore, predicting the ultimate capacity of a cold-formed steel member when instability occurs is the key step in its design. Research on the stability of cold-formed steel

members can be traced back to the 1940s (Qin and Chen 2016). In terms of experimental research, Elgaaly *et al.* (1991) tested more than 107 compression members to investigate the influence of the slenderness ratio and constraint conditions. The results demonstrated that the capacity of the members with large slenderness ratio is very close to the numerical values calculated by the classical Euler's formula. However, when the slenderness ratio is less than 85, Euler's formula cannot yield a good prediction. In this case, eccentric loading has a more significant effect on the capacity than the constraint condition. Later, Schafer and Pekoz (1998) discussed the theoretical calculation method for determining the ultimate capacity of cold-formed steel members with different slenderness ratios. Based on theoretical and experimental results, design methods for cold-formed members with equal-angle or singly symmetric sections were developed by Dhanalakshmi and Shanmugam (2001) and Young and Rasmussen (1999) respectively. Deeper insights were explored by Narayanan and Mahendran (2003). With the development of computer technology, finite element analysis supplied another tool for investigating the mechanical behavior of cold-formed steel members. Using finite element analysis together the experimental data, Zhou and Young (2007) and Huang and Young (2013) further improved the design method for the cold-formed steel members. With the combination of finite element analysis and model updating technique, Wang *et al.* (2016) developed a method for evaluating the performance of a transmission tower structure. Based on these fundamentals, the behavior of high strength steel (Feng *et al.* 2017, Pournara *et al.* 2017 and Li *et al.* 2016) has also been discussed recently.

The previous studies on the ultimate capacity of cold-formed steel members mostly focused on members subjected to concentric loading. However, there are six

*Corresponding author, Assistant Professor
E-mail: tzy@bjut.edu.cn

^aPh.D. candidate
E-mail: hjk@epri.sgcc.com.cn

^bAssistant Professor
E-mail: zhaoxu@bjut.edu.cn

^cAssociate Professor
E-mail: mahua@bjut.edu.cn

^dProfessor
E-mail: lizb@bjut.edu.cn

different boundary conditions in a transmission tower. At present two design codes are used for transmission tower design in China: Guide for Design of Steel Transmission Towers (GDST) (Jackman 1984) and Technical Regulations for Design of Tower and Pole Structures for Overhead Transmission Lines (TRTPS) (DL/T5154-2002). However, they do not address the use of cold-formed steel. Therefore, to grasp the bearing capacity of cold-formed steel under different boundary conditions in transmission towers, a total of 105 compression members were tested statically. A finite element analysis method was also developed and calibrated using the experimental data, and additional cases beyond the tested members were investigated with finite element analysis. The design methods for the members in transmission towers were modified based on the experimental and numerical results.

2. Commonly used design methods

As mentioned in Section 1, the GDST and the TRTPS are the commonly used design codes for transmission towers in China. The bearing capacity of a steel member subjected to concentric load is expressed as follows

$$F_{cr} = \phi A_e f_y \quad (1)$$

where ϕ is the stability factor, A_e is the equivalent section area, and f_y is the yield strength of the selected steel. In this equation, the stability factor (ϕ) is related to the slenderness ratio (λ). The relationship between these two coefficients is presented with a ϕ - λ table in the GDST and TRTPS. In the Technical Code for Cold-formed Thin-wall Steel Structures (CMC, 2002), the ϕ - λ curve is governed by Eqs. (2) and (3). When $0 < \lambda_0 \leq 1.2$

$$\phi = 1.0 - 0.071\lambda_0 - 0.209\lambda_0^2 \quad (2)$$

When $1.2 < \lambda_0 \leq 2.5$

$$\phi = 0.046 + 0.506\lambda_0^{-1} + 0.211\lambda_0^{-2} \quad (3)$$

In Eqs. (2) and (3), λ_0 is the equivalent slenderness ratio, which is expressed as follows

$$\lambda_0 = \frac{\lambda}{\pi} \sqrt{\frac{f_y}{E}} \quad (4)$$

where E is the Young's modulus of the steel.

In the GDST and TRTPS, two additional types of boundary conditions are considered, but axis compression loading is excluded. One included condition is eccentric loading, which results from one angle of the cold-formed steel connected in the construction of the transmission tower. The other is end restraint, which is caused by cold-formed steel fixed by two and more bolts. To consider the effects of eccentric loading and end restraint, while using the same design method as for concentric loading, only the slenderness ratio (λ) is adjusted in the design. The GDST and TRTPS specify that when λ is less than 120 it is necessary to consider eccentric loading; when λ is larger

than 120, end restraint cannot be neglected. After considering the influence of eccentric loading and end restraint, λ is replaced by $K\lambda$ in Eq. (4). In the GDST, the K values for different boundary conditions are as follows:

Boundary condition 1 (B1): Concentric loading at two ends. For example, the two legs (See Fig. 1) at the two ends of a member are both fixed by bolts. In this case

$$K = 1 \quad (5)$$

Boundary condition 2 (B2): Concentric loading at one end and eccentric loading at the other end. For example, two legs at one end are fixed by bolts, and one leg at the other end is fixed by bolts. In this case

$$K = 0.75 + \frac{30}{\lambda} \quad (6)$$

Boundary condition 3 (B3): Eccentric loading at two ends. For example, one leg at each end is fixed by bolts. In this case

$$K = 0.5 + \frac{60}{\lambda} \quad (7)$$

Boundary condition 4 (B4): Without end restraint at the two ends. For example, one bolt is used for each end. In this case

$$K = 1 \quad (8)$$

Boundary condition 5 (B5): Without end restraint at one end and with end restraint at the other end. For example one bolt is used at one end and two or more bolts are used for the other end. In this case

$$K = 0.762 + \frac{28.6}{\lambda} \quad (9)$$

Boundary condition 6 (B6): With end restraint at two ends. For example, two or more bolts are used at the two ends. In this case

$$K = 0.615 + \frac{46.2}{\lambda} \quad (10)$$

In TRTPS, the expression of K is the same as in the GDST for B1 to B4. B5 and B6 are, respectively, as follows

$$K = 0.9 + \frac{11.89}{\lambda} \quad (11)$$

and

$$K = 0.82 + \frac{21.64}{\lambda} \quad (12)$$

3. Experimental testing

3.1 Specimens details

The purpose of the test was to determine the design method for cold-formed steel with different boundary conditions in transmission towers. The section L90°-

Table 1 Boundary conditions and slenderness ratios for various specimens

Boundary condition	Slenderness ratio
B1	50,60,70,80,90,100,110
B2	60,70,80,90,100,110,120
B3	60,70,80,90,100,110,120
B4	120,130,150,170,190
B5	120,140,160,180
B6	120,140,160,180,200

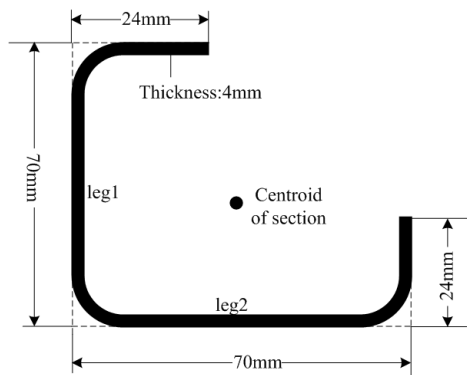


Fig. 1 Section of the tested specimen

$70 \times 70 \times 24 \times 4$ (unit: mm) was chosen. The steel used was Chinese Grade 345 (CMC, 2002); the yield strength and Young's modulus (442 MPa and 210 GPa, respectively) were measured from coupon test results. As known from the specifications in the GDST and TRTPS, when λ is less than 120, it is necessary to consider eccentric loading; when λ is larger than 120, end restraint cannot be neglected. Hence, for boundary conditions B1 to B3, the value of λ is below 120, while for boundary conditions B4 to B6, the value of λ is above 120. The specific parameters of the tested specimens are presented in Table 1. To eliminate uncertainties in the test, three specimens were designed for each test case. A total of 35 test cases, including 105 specimens, were conducted in this work.

3.2 Loading system

It was necessary to simulate two types of boundary conditions: eccentric (or concentric) loading and end restraint. To implement the eccentric (or concentric) loading, the system shown in Fig. 2 was specially designed. In this loading system, a special connection (displayed in Fig. 2(b), (c)) was designed for each end of the specimen. The end of the specimen was fixed on a junction plate with a stopper, a steel block, and clamp bolts. This allowed the specimen to be changed easily. On the other side of the junction plate, a connecting trough was used, which could be used to adjust the expected loading point. A dowel bar was connected with the loading jack, so that the eccentric or concentric loading could be implemented successfully for each end.

To simulate end restraint experimentally, a connector (as shown in Fig. 3) for joining the specimen and the jack was designed. Boundary conditions B4 to B6 were implemented

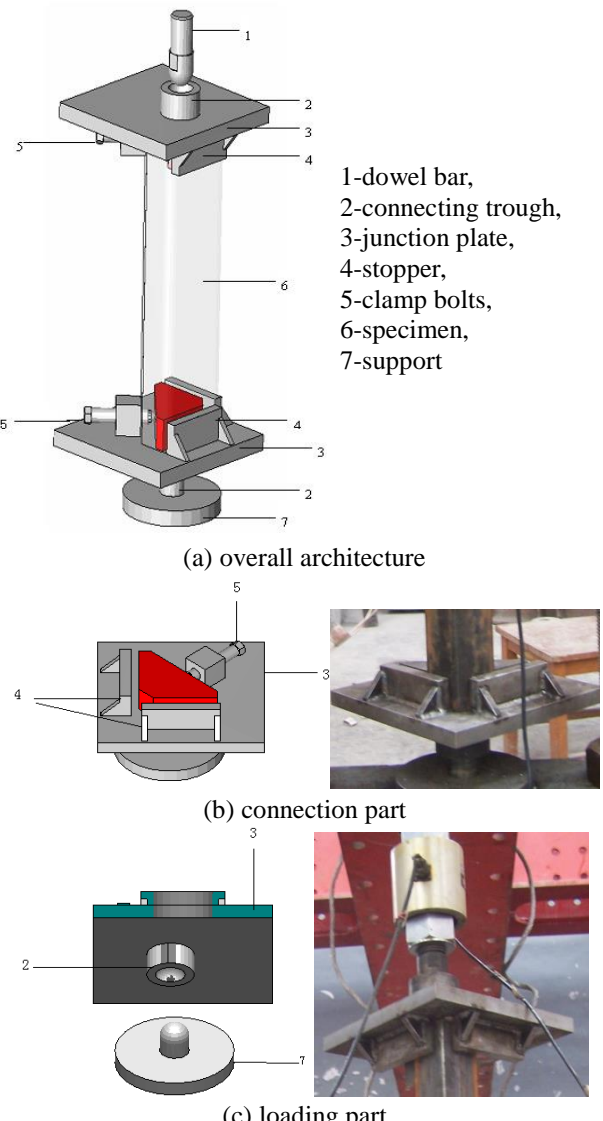


Fig. 2 Test setup for condition B1 to B3

when one or two bolts were installed at each end. The photograph of the test set-up for the simulation of eccentric loading and end restraint can be seen in Fig. 4 and Fig. 5, respectively.

The axial load was applied to the specimen at the beginning of the test and was increased to a velocity of 0.5 kN/s before instability occurred. When the loading was close to the buckling bearing capacity predicted by finite element analysis, and the loading velocity was increased to 0.05 kN/s until the tested specimen failed.

Fig. 6 shows the failure states of typical specimens. The failure states demonstrated that these specimens all failed by global buckling, including flexural buckling and flexural-torsional buckling. This also was verified by the strain response (See Fig. 7) measured in the test. As can be seen from Fig. 7(a), for the specimens subjected to concentric loading, the strain response at the symmetric location was asymmetric, caused by torsional buckling. A comparison of Figs. 7(a) and 7(b) shows that the moment resulting from eccentric loading or end restraint only

affected the mechanical properties of the specimen in the elastic range. Once the strain response of the middle section approached $1500 \mu\epsilon$, the strain increased and the load decreased rapidly. This indicates that buckling occurred and the specimen failed. The peak load measured during the test was defined as the ultimate capacity. The average value of the three specimens for one case was regarded as the capacity of the calculated slenderness ratio. The capacities of all tested specimens are included in Table 1, together with the comparison between the experimental values and the predicted values from the GDST and TRTPS, which is characterized by the ratio of the predicted and the measured capacity of the specimen.

The experimental results shown in Table 2 indicate that in some cases the comparison ratio is less than one, which means the capacity of the cold-formed steel member was underestimated by the GDST and TRTPS. In other cases, the ratio is greater than one, demonstrating that the capacity was overestimated. Generally, the predicted value from the GDST and TRTPS cannot describe the capacity of the cold-formed steel member under different boundary conditions in transmission towers. For the boundary conditions B1 and B2, the errors between the experimental results and the two codes were more than 10%, with a maximum error of 41.8%. For the boundary conditions B4, B5, and B6, the GDST showed relatively small errors (less than 10%), except in a few cases. However, in these cases, the TRTPS yielded large errors (generally greater than 30%). The boundary condition B3 was the only one, which could be predicted by TRTPS, with small errors in most cases. Overall, the use of the existing guides resulted in relatively large design errors for cold-formed steel members in transmission towers in China.



Fig. 3 Connection parts for boundary conditions B4 to B6



Fig. 4 Test photo for boundary conditions B1 to B3

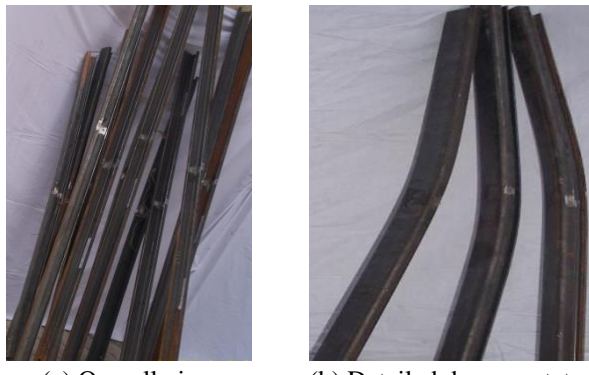


Fig. 5 Test photo for boundary conditions B4 to B6

Table 2 Comparison of test results and predicted values from GDST and TRTPS

Boundary condition :B1							
Slenderness ratio	50	60	70	80	90	100	110
Measured(kN)	210.27184.95170.40157.47138.15116.87100.07						
Comparison	GDST	0.77	0.78	0.74	0.73	0.77	0.85
	TRTPS	0.84	0.86	0.82	0.76	0.74	0.75
Boundary condition :B2							
Slenderness ratio	60	70	80	90	100	110	120
Measured (kN)	139.53124.99114.36103.54	97.28	89.35	79.41			
Comparison	GDST	0.79	0.84	0.88	1.02	1.04	1.12
	TRTPS	0.82	0.84	0.84	0.91	0.87	0.88
Boundary condition :B3							
Slenderness ratio	60	70	80	90	100	110	120
Measured (kN)	117.05101.34	93.74	85.37	76.45	70.35	63.82	
Comparison	GDST	1.23	1.41	1.42	1.38	1.40	1.39
	TRTPS	0.88	0.94	0.94	0.95	0.99	1.00
Boundary condition :B4							
Slenderness ratio	120	130	150	170	190		
Measured (kN)	69.74	68.41	56.95	48.44	41.50		
Comparison	GDST	1.29	1.12	1.01	0.93	0.87	
	TRTPS	0.93	0.83	0.77	0.72	0.69	
Boundary condition :B5							
Slenderness ratio	120	140	160	180			
Measured (kN)	95.89	76.99	62.05	51.18			
Comparison	GDST	0.92	0.92	0.92	0.92		
	TRTPS	0.68	0.67	0.66	0.66		
Boundary condition :B6							
Slenderness ratio	120	140	160	180	200		
Measured (kN)	94.64	75.54	62.46	54.67	45.52		
Comparison	GDST	0.94	0.98	0.99	0.96	0.99	
	TRTPS	0.69	0.69	0.68	0.65	0.65	

Note: the values in the comparison row are the ratios of the values predicted by GDST or TRTPS and the measured capacity of the specimen



(a) Overall view (b) Detailed damage states

Fig. 6 Failure states of the tested specimens

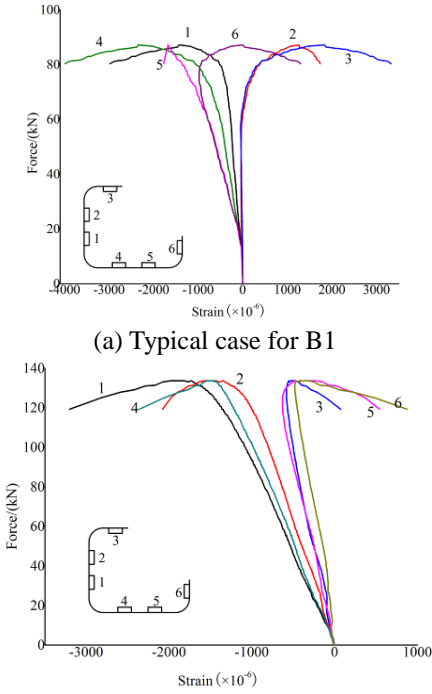
(a) Typical case for B1
(b) Typical case for B2 to B6

Fig. 7 Strain response

4. Numerical simulation

4.1 General

A considerable number of experimental results are presented in Section 3, but they are not adequate to reach a quantitative conclusion for transmission tower design under different boundary conditions. To amass more data at a low cost, finite element analysis (FEA) was also used. In order to simulate the actual behavior of cold-formed steel under different boundary conditions in transmission towers, the following main components need to be modeled properly: the bearing plate, the cold-formed steel section, the fixed base plate. The non-linear finite element analysis program ANSYS (Narayanan and Mahendran 2003) version 12.0 was used to simulate the nonlinear behavior of cold-formed steel under different boundary conditions in transmission towers. In the finite element model (FEM), the measured

cross-sectional dimensions and material properties obtained from the coupon test were used. The model was based on the centreline dimensions of the cross-sections. The corners of the cold-formed steel sections were accurately modeled.

4.2 Element type and mesh

The bearing plate and the fixed plate steel base plate were regarded as rigid plates through assigning an infinite Young modulus to their material. In the simulation of this type of thin-walled member, buckling behavior is the key feature. Hence, the Shell 181 element was selected, which is tailored for buckling behaviour. The Shell 181 element is a four-node doubly curved thin or thick shell element with reduced integration, hourglass control and finite membrane strains. This element has six degrees of freedom per node and provides accurate simulation to the buckling behavior. The finite element mesh used in the model was investigated by varying the size of the elements in the cross-section to provide both accurate results and less computational time. The finite element mesh sizes were set to 2 mm for the cross-section (x and y direction), and 5 mm for the length (z direction).

4.3 Boundary condition

Following the test procedure, there were two types of boundary condition. Eccentric loading needs to be simulated boundary conditions B1 to B3, while the end constraint needs to be simulated boundary conditions B4 to B6. In the simulation, the bearing plate and the fixed plate were fixed with the specimen. All the boundary conditions were implemented through the bearing plate and the fixed flat. As in the previous tests, eccentric loading was simulated by changing the offset of the loading point from the centroid of section as shown in Fig. 1. The constraint release was used to simulate the end restraint.

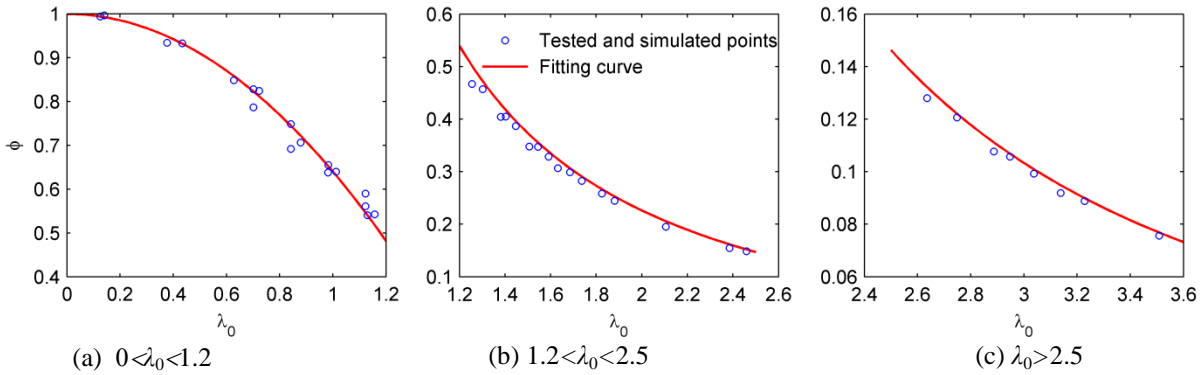
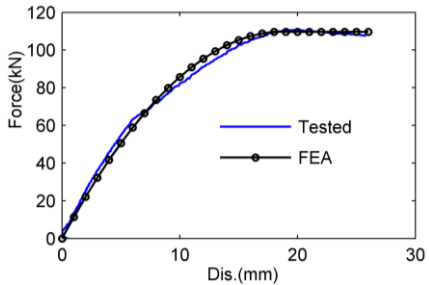
4.4 Material modelling

For the stress-strain curves, the material behaviour provided by ANSYS for bi-linear stress-strain curves was adopted. The measured stress-strain curves for flat portions of the specimens in coupon test were used in the analysis. The first part of the bi-linear curve represents the elastic part up to the proportional limit stress with measured Young's modulus and Poisson's ratio equal to 0.3. The measured yield point is used to define the nonlinear part.

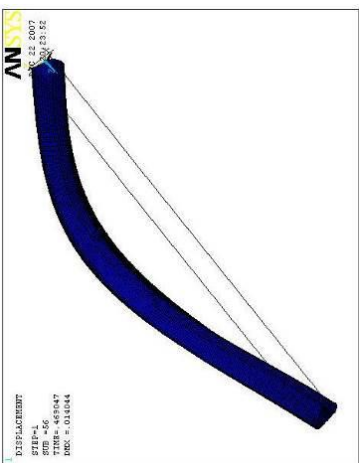
4.5 Verification of finite element model

The loading method used in the FEA was identical to that used in the tests. The force control method was used for the analysis of the cold-formed steel under different boundary conditions in transmission towers.

The deformation curve for boundary condition B1 with $\lambda=60$ is presented in Fig. 8. It shows that the finite element prediction properly described the mechanical behavior observed in the test. This was also proved by the failure mode, shown in Fig. 9.

Fig. 10 Fitted ϕ - λ_0 curve for cold-formed steel member subjected to concentric loadingFig. 8 Deformation curve for boundary condition B1 with $\lambda=60$ 

(a) Experiment



(b) Finite element analysis

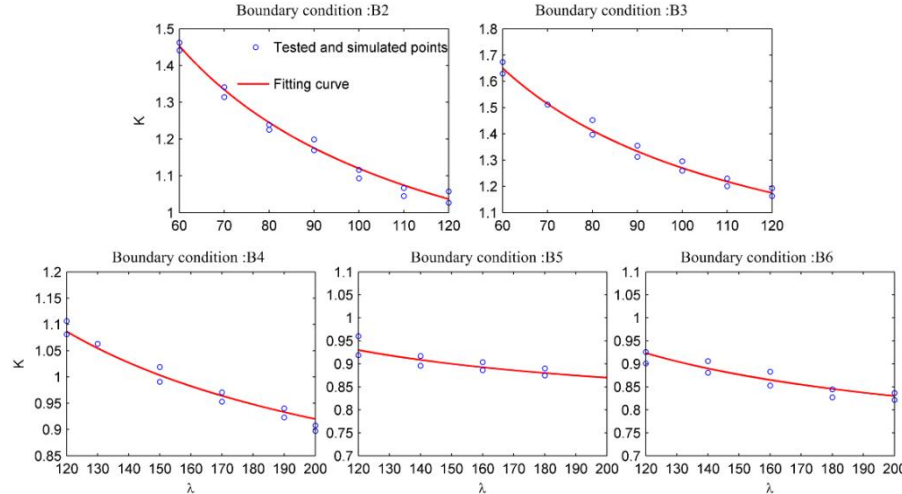
Fig. 9 Failure mode for boundary condition B2 with $\lambda=60$

To verify its effectiveness, all the test cases from Section 3 were simulated using FEA; the analytical results (F_a) are summarized in Table 3, along with the comparative errors with the experimental results (F_e). The comparison between the analytical and experimental results shows that the errors were all less than 10%, and most of them were less than 5%. This indicates that the finite element model used here can be used to extend the experimental data.

Table 3 Comparison of experimental and FEA results

Boundary condition: B1							
Slenderness ratio	50	60	70	80	90	100	110
Simulated (kN)	221.41	200.02	175.03	149.76	125.30	108.17	92.65
Comparison(%)	-5.3	-8.1	-2.7	4.9	9.3	7.4	7.4
Boundary condition: B2							
Slenderness ratio	60	70	80	90	100	110	120
Simulated (kN)	142.88	129.23	116.47	99.36	93.91	86.33	75.48
Comparison (%)	-2.4	-3.4	-1.8	4.0	3.5	3.4	5.0
Boundary condition: B3							
Slenderness ratio	60	70	80	90	100	110	120
Simulated (kN)	111.96	102.74	87.79	80.83	72.78	67.44	61.02
Comparison (%)	4.3	-1.4	6.3	5.3	4.8	4.1	4.4
Boundary condition: B4							
Slenderness ratio	120	130	150	170	190		
Simulated (kN)	72.63	64.95	54.08	46.76	39.98		
Comparison (%)	-4.1	5.1	5.0	3.5	3.7		
Boundary condition: B5							
Slenderness ratio	120	140	160	180			
Simulated (kN)	89.05	73.95	59.90	49.53			
Comparison (%)	7.1	3.9	3.5	3.2			
Boundary condition: B6							
Slenderness ratio	120	140	160	180	200		
Simulated (kN)	99.07	79.31	66.46	56.78	47.19		
Comparison (%)	-4.7	-5.0	-6.4	-3.9	-3.7		

Note: the values in the comparison row are the errors between the experimental (F_e) and numerical (F_a) results, $100*(F_a - F_e)/F_e$.

Fig. 11 Fitted K - λ curve for boundary conditions B2 to B6

5. Suggested design methods

As discussed in Section 3, the GDST and TRTPS significantly overestimated or underestimated the capacity of the cold-formed steel member in transmission towers. The suggested design methods for improving estimation accuracy for the capacity of cold-formed steel members are discussed in this section.

The GDST and TRTPS do not consider cold-formed steel. Technical code for cold-formed thin-wall steel structures (Feng *et al.* 2017) is specialized for cold-formed steel, but it does not include all the boundary conditions used in transmission towers. Hence, based on the experimental and analytical results, Eqs. (2) and (3) were used for curve fitting to describe the relation of $\phi\lambda_0$ for the boundary condition B1. The fitting curves, together with experimental and analytical, results are plotted in Fig. 10. It was noted in Section 2 that Eqs. (2) and (3) are suitable for $\lambda_0 < 2.5$. As can be seen in Figure 10(c), the trend of data for $\lambda_0 > 2.5$ is the same as for $1.2 < \lambda_0 \leq 2.5$. Therefore, the same formula used for $1.2 < \lambda_0 \leq 2.5$ was used for $\lambda_0 > 2.5$. The design curve for the boundary condition B1, derived from curve fitting, is shown in Eq. (13). The comparative results displayed in Fig. 10 showed that Eq. (13) can describe the $\phi\lambda_0$ curve accurately

$$\begin{cases} \phi = 1 - 0.36\lambda_0^2 & 0 < \lambda_0 \leq 1.2 \\ \phi = -0.1 + 0.49\lambda_0^{-1} + 0.34\lambda_0^{-2} & 1.2 < \lambda_0 \leq 2.5 \\ \phi = 0.03\lambda_0^{-1} + 0.83\lambda_0^{-2} & \lambda_0 > 2.5 \end{cases} \quad (13)$$

The same strategy that was used in the GDST and TRTPS was adopted here to manage boundary conditions B2 to B6. To diminish the errors caused by the GDST and TRTPS, the K - λ curves for the boundary conditions B2 to B6 were modified based on the experimental and analytical points by curve fitting. The fitting results were as follows:

Boundary condition B2: $K=0.62+50/\lambda$,
 Boundary condition B3: $K=0.7+57/\lambda$,
 Boundary condition B4: $K=0.67+50/\lambda$,
 Boundary condition B5: $K=0.78+18/\lambda$,

Table 4 Comparison of experimental results and the suggested design methods

Boundary condition :B2							
	50	60	70	80	90	100	110
Predicted (kN)	219.73	198.93	174.35	145.99	133.92	112.73	96.24
Comparison (%)	-4.5	-7.6	-2.3	7.3	3.1	3.5	3.8
Boundary condition :B2							
	60	70	80	90	10	110	120
Predicted(kN)	140.97	126.08	113.48	102.70	93.38	85.25	78.11
Comparison (%)	-1.0	-0.9	0.8	0.8	4.0	4.6	1.6
Boundary condition :B3							
	60	70	80	90	10	110	120
Predicted (kN)	114.61	102.37	91.99	83.08	75.36	68.61	62.67
Comparison (%)	2.08	-1.02	1.87	2.68	1.43	2.47	1.80
Boundary condition :B4							
	120	130	150	170	190		
Predicted (kN)	71.98	65.89	55.66	47.39	40.59		
Comparison (%)	-3.2	3.7	2.3	2.2	2.2		
Boundary condition :B5							
	120	140	160	180			
Predicted (kN)	93.94	75.16	61.25	50.58			
Comparison (%)	2.0	2.4	1.3	1.2			
Boundary condition :B6							
	120	140	160	180	200		
Predicted (kN)	95.08	77.89	64.79	54.51	46.24		
Comparison (%)	-0.5	-3.1	-3.7	0.3	-1.6		

Boundary condition B6: $K=0.69+28/\lambda$.

The comparison of the fitted curves and the experimental and analytical points is plotted in Figure 11. It shows that the fitted curves agree well with the experimental and analytical results.

To evaluate the performance of the suggested design methods, the capacities of the tested specimens were calculated using the fitted equation. The calculated values are listed in Table 4, together with the comparative error with the experimental results. The errors were all less than 10%, and most of them were less than 5%. This indicates the suggested design method can yield better predictions for the bearing capacity of cold-formed steel in transmission towers than the existing guides.

6. Conclusions

There is not a special design code for cold-formed steel used under different boundary conditions in transmission towers. To investigate the accuracy of the commonly used design codes, a series of cold-formed steel members were tested experimentally. The comparison of the test results and the results predicted by the current design codes showed a significant divergence.

To get more test data at a low cost, the performance of coupled members was simulated through finite element analysis. Based on the experimental and analytical results, the design methods were modified for the six different boundary conditions that exist in transmission towers. The comparative results showed that the suggested design methods can yield better predictions for the bearing capacity of cold-formed steel in transmission towers than the current codes.

Acknowledgments

The authors would like to thank the sponsors, the State Grid Corporation of China and the National Natural Science Foundation of China (51408378).

Reference

- Bathon, L., Mueller, W.H. and Kempner, L. (1993), "Ultimate load capacity of single steel angles", *J. Struct. Eng.*, **119**(1), 279-300.
- CMC. (2002), Technical code of cold-formed thin-wall steel structures(GB 50018-2002), China Ministry of Construction. (in Chinese)
- Dhanalakshmi, M. and Shanmugam, N.E. (2001), "Design for openings in equal-angle cold-formed steel stub columns", *Thin-Wall. Struct.*, **39**(2), 167-187.
- DL/T5154-2002 (2002), Technical Regulation of design for tower and pole structures of overhead transmission line, China Electric Power Press, Beijing. (in Chinese)
- Elgaaly, M., Dagher, H. and Davids, W. (1991), "Behavior of single-angle-compression members", *J. Struct. Eng.*, **117**(12), 3720-3741.
- Feng, P., Zhang, Y.H., Hu, L.L. and Gong, D. (2017), "Buckling of piecewise member composed of steel and high-strength materials in axial compression", *Thin-Wall. Struct.*, **110**, 62-74.
- Huang, Y.N. and Young, B. (2013), "Experimental and numerical investigation of cold-formed lean duplex stainless steel flexural members", *Thin-Wall. Struct.*, **73**, 216-228.
- Jackman, D.E. (1984), Guideline for Transmission Line Structural Loading, Committee on Electrical Transmission Structures, American Society of Civil Engineers, ASCE, New York.
- Jiang, J., Sun, H.F., An, N., Shi, Y., Zhang, Z.Y. and Jing, Y.M. (2014), "Study on applicable conditions of transmission line tower foundation natural grounding in less thunderstorm days region in northwest China", *International Conference on Lightning Protection*, Shanghai, China, October.
- Kennedy, J.B. and Murty, M.K.S. (1972), "Buckling of steel angle and tee struts", *J. Struct. Div.*, **98**(ST11), 2507-2522.
- Li, T.J., Li, G.Q., Chan, S.L. and Wang, Y.B. (2016), "Behavior of Q690 high-strength steel columns: Part 1: Experimental investigation", *J. Constr. Steel Res.*, **123**, 18-30.
- Li, Z., He, M.J., Li, M.H. and Lam, F. (2014), "Damage assessment and performance-based seismic design of timber-steel hybrid shear wall systems", *Earthq. Struct.*, **7**(1), 101-117.
- Narayanan, S. and Mahendran, M. (2003), "Ultimate capacity of innovative cold-formed steel columns", *J. Constr. Steel Res.*, **59**(4), 489-508.
- Nashid, H., Clifton, C., Ferguson, G., Hodgson, M., Seal, C. and Choi, J.H. (2015), "Relationship between hardness and plastically deformed structural steel elements", *Earthq. Struct.*, **8**(3), 619-637.
- Pournara, A.E., Karamanos, S.A., Mecozzi, E. and Lucci, A. (2017), "Structural resistance of high-strength steel CHS members", *J. Constr. Steel Res.*, **128**, 152-165.
- Qin, Y. and Chen, Z.H. (2016), "Research on cold-formed steel connections: A state-of-the-art review", *Steel Compos. Struct.*, **20**(1), 21-41.
- Rosario-Galanes, O. and Godoy, L.A. (2014), "Modeling of wind-induced fatigue of cold-formed steel sheet panels", *Struct. Eng. Mech.*, **49**(2), 237-259.
- Schafer, B.W. and Pekoz, T. (1998), "Computational modeling of cold-formed steel: characterizing geometric imperfections and residual stresses", *J. Constr. Steel Res.*, **47**(3), 193-201.
- Shahi, R., Lam, N., Gad, E. and Wilson, J. (2013), "Protocol for testing of cold-formed steel wall in regions of low-moderate seismicity", *Earthq. Struct.*, **4**(6), 629-647.
- Wang, F.Y., Xu, Y.L. and Zhan, S. (2016), "Multi-scale model updating of a transmission tower structure using Kriging meta-method", *Struct. Control Hlth. Monit.*, 1-16.
- Yang, F.L., Han, J.K., Yang, J.B. and Li, Z. (2009), "Study on the application of weathering and cold-formed steel in transmission tower", *Asia-Pacific Power and Energy Engineering Conference*, Wuhan, China, December.
- Yang, F.L., Han, J.K., Yang, J.B. and Li, Z.B. (2011), "Study on the buckling behaviour of cold-formed angles in transmission towers", *Int. J. Steel Struct.*, **11**(4), 495-508.
- Yang, S., Li, H., Zhou, W.J. and Yu, J.H. (2014), "Lightning current waveform observed on transmission line and lightning tower in China", *International Conference on Lightning Protection*, Shanghai, China, October.
- Young, B. and Rasmussen, K.J.R. (1999), "Behaviour of cold-formed singly symmetric columns", *Thin-Wall. Struct.*, **33**(2), 83-102.
- Zhou, F. and Young, B. (2007), "Experimental and numerical investigations of cold-formed stainless steel tubular sections subjected to concentrated bearing load", *J. Constr. Steel Res.*, **63**(11), 1452-1466.

KT